Phase diagram of the ferromagnetic shape memory alloys $Ni_2MnGa_{1-x}Co_x$

T. Kanomata,[1,2] S. Nunoki,[1] K. Endo,[1,2] M. Kataoka,[3] H. Nishihara,[4] V. V. Khovaylo,[5] R. Y. Umetsu,[6,*] T. Shishido,[6] M. Nagasako,[2] R. Kainuma,[2] and K. R. A. Ziebeck[7]

[1]*Faculty of Engineering, Tohoku Gakuin. University, Tagajo 985-8537, Japan*

[2]*Department of Material Science, Graduate School of Engineering, Tohoku University, Sendai 980-8579, Japan*

[3]*Department of Basic Sciences, Faculty of Science and Engineering, Ishinomaki Senshu University, Ishinomaki 986-8580, Japan*

[4]*Faculty of Science and Technology, Ryukoku University, Otsu 520-2194, Japan*

[5]*National University of Science and Technology MISiS, Moscow 119049, Russia*

[6]*Institute for Materials Research, Tohoku University, Sendai 980-8577, Japan*

[7]*Department of Physics, Cavendish Laboratory, University of Cambridge, CB3, 0HE, United Kingdom*

(Received 14 November 2011; revised manuscript received 14 March 2012; published 11 April 2012)

Permeability, magnetization, and differential scanning calorimetry measurements are carried out on the ferromagnetic shape memory alloys $Ni_2MnGa_{1-x}Co_x$ ($0 \leqslant x \leqslant 0.20$). On the basis of the experimental results, the phase diagram in the temperature-concentration plane is determined. The determined phase diagram is spanned by a paramagnetic austenite (Para-A) phase, paramagnetic martensite phase, ferromagnetic austenite phase, ferromagnetic martensite (Ferro-M) phase, and a premartensite phase. The measurements show that a magnetostructural transition between the Para-A and Ferro-M phases does not appear in this alloy system. The phase diagram is discussed using phenomenological Landau theory.

DOI: 10.1103/PhysRevB.85.134421 PACS number(s): 75.50.−y, 68.35.Rh, 64.60.Ej, 81.30.Kf

I. INTRODUCTION

Recently, much activity has been devoted to the study on ferromagnetic shape memory alloys (FSMAs), which exhibit both the ferromagnetic and structural transitions. The interplay of the two phase transitions causes some exotic phenomena, which make these alloys candidates for functional materials. In fact, a large magnetic-field-induced strain by the rearrangement of twin variants in the martensite phase[1,2] is used in magnetomechanical actuators. Moreover, a large magnetocaloric effect (MCE) accompanied by a magnetostructural transition, where both the ferromagnetic and structural transition occur together, has been expected to be useful for devices.[3–8] Among many FSMAs, Ni-Mn-based alloys have attracted much attention from researchers because of their rich phenomena.

The stoichiometric Heusler alloy Ni_2MnGa orders ferromagnetically at the Curie temperature $T_C \approx 365$ K.[9,10] On cooling below a martensitic transition temperature $T_M \approx 200$ K, a superstructure forms.[9,10] Recently, Kataoka *et al.* carried out magnetization, initial permeability, and differential scanning calorimetric (DSC) measurements on the FSMAs $Ni_2Mn_{1-x}Cu_xGa$ ($0 \leqslant x \leqslant 0.4$).[11] On the basis of the results, the phase diagram in the temperature-concentration plane was determined for this alloy system. It was found that for $Ni_2Mn_{1-x}Cu_xGa$ ($0 \leqslant x \leqslant 0.4$) alloys the magnetostructural transitions between the paramagnetic austenite (Para-A) phase and the ferromagnetic martensite (Ferro-M) phase occur in the concentration range $0.23 \leqslant x \leqslant 0.30$. Furthermore, the characteristics of the phase diagram of $Ni_2Mn_{1-x}Cu_xGa$ ($0 \leqslant x \leqslant 0.4$) alloys were found to be closely similar to that of $Ni_{2+x}Mn_{1-x}Ga$ ($0 \leqslant x \leqslant 0.36$).[12,13] Measurements of the MCE for $Ni_2Mn_{1-x}Cu_xGa$ alloys have been reported by many authors.[14–16] In order to understand the phase diagram of $Ni_2Mn_{1-x}Cu_xGa$ ($0 \leqslant x \leqslant 0.30$) alloys, Kataoka *et al.* developed the analysis using the Landau-type phenomenological free energy as a function of the martensitic distortion and the magnetization.[11] Their analysis showed that the biquadratic coupling term, together with a higher-order coupling term, of the martensitic distortion and the magnetization plays an important role in the interplay between the martensite phase and the ferromagnetic phase. More recently, parallel measurements were carried out on the FSMAs $Ni_2MnGa_{1-x}Cu_x$ ($0 \leqslant x \leqslant 0.25$).[17] On the basis of the results, the phase diagram in the temperature-concentration plane was determined for $Ni_2MnGa_{1-x}Cu_x$ ($0 \leqslant x \leqslant 0.25$) alloys. It was shown that the phase diagram of $Ni_2MnGa_{1-x}Cu_x$ ($0 \leqslant x \leqslant 0.25$) alloys was very similar to those of $Ni_{2+x}Mn_{1-x}Ga$ ($0 \leqslant x \leqslant 0.36$) and $Ni_2Mn_{1-x}Cu_xGa$ ($0 \leqslant x \leqslant 0.4$) alloys. Both the martensitic transition and Curie temperatures of $Ni_2MnGa_{1-x}Cu_x$ ($0 \leqslant x \leqslant 0.25$) alloys merged together in samples with $0.12 \leqslant x \leqslant 0.14$.

It is well-known that the structural and magnetic transitions of Ni-Mn-based FSMAs depend strongly on the valence electron concentration. On the basis of first-principles calculations, Entel *et al.* investigated the physical properties of $Ni_2MnGa_{0.875}Co_{0.125}$.[18] They estimated the differences in magnetic moment and total energy between the austenite and martensite phases and found the energy of the martensite phase with the tetragonal distortion is much lower than that of the austenite phase with the $L2_1$ structure. For the Ni-Mn-Ga FSMAs, the low values of both transition temperatures (T_C and T_M) and its poor mechanical properties limit the use of these alloys in practical devices. The calculation showed also that the addition of small amounts of Co to the Ni-Mn-Ga FSMAs is an efficient way to increase both T_C and T_M of such alloys.[18] However, on the other hand, experimental studies of the correlation between composition and phase transition temperatures in Co-modified Ni-Mn-Ga FSMAs[14,19–43] were done mostly for the alloy systems $Ni_{2-x}Co_xMnGa$ and $Ni_2Mn_{1-x}Co_xGa$, or nonstoichiometric Ni-Mn-Co-Ga alloys,[14,19–43] but those on $Ni_2MnGa_{1-x}Co_x$ alloys, which can clarify the effect of substitution of Ga by Co with conserving the stoichiometries of Ni and Mn cations, have scarcely ever been reported.

In this paper, the structural and magnetic properties of $Ni_2MnGa_{1-x}Co_x$ ($0 \leqslant x \leqslant 0.20$) alloys are examined experimentally by measuring the permeability, magnetization, and DSC. The phase diagram obtained for this alloy system is compared with the already reported phase diagrams of $Ni_{2+x}Mn_{1-x}Ga$ and $Ni_2Mn_{1-x}Cu_xGa$ exhibiting the magnetostructural transition and also with the phase diagram of $Ni_{50.6}Mn_{24.4}Ga_{25-x}Co_x$ ($0 \leqslant x \leqslant 6.4$)[40] whose composition is not far from that of the alloy system in the present study. The phase diagram of the last alloy system has been already predicted by Soto-Parra *et al.*[40] on the basis of a limited number of their observed data on the magnetic and structural transition temperatures. Their phase diagram looks very peculiar compared with those of other alloy systems and does not show any finite concentration region of the occurrence of the magnetostructural transition. In our study, therefore, we aim also to investigate such a possible peculiar phase diagram of $Ni_2MnGa_{1-x}Co_x$ by measuring the transition temperatures of a sufficient number of the alloys with different concentrations of x. The obtained phase diagram is analyzed within the framework of the phenomenological Landau theory, which was proposed for $Ni_2Mn_{1-x}Cu_xGa$.[11] Through this analysis, the reason for different features of the phase diagrams will be clarified.

II. EXPERIMENTAL PROCEDURE

The polycrystalline $Ni_2MnGa_{1-x}Co_x$ ($0 \leqslant x \leqslant 0.20$) alloys were prepared by the repeated melting of the appropriate quantities of constituent elements, namely 99.99% pure Ni and Mn, 99.9% pure Co, and 99.9999% pure Ga, in an argon arc furnace. All reaction products were sealed in evacuated silica tubes, heated at 1073 K for 3 days, and then at 873 K for 1 day before being quenched into water. The phase characterizations of the samples were carried out by x-ray powder diffraction measurements using Cu-Kα radiation. The observed x-ray diffraction patterns were analyzed using the Rietveld profile refinement technique. The Curie temperature and martensitic transition temperatures were determined by an ac transformer method in which the primary and secondary coils were wound around a cylindrical sample of diameter $\sim$1 mm and length $\sim$10 mm. When an ac current of a constant amplitude flows in the primary coil, the voltage induced in the secondary coil is directly proportional to the initial permeability. The frequency of the ac magnetic field is 1 kHz. The magnetization M data were collected using a commercial superconducting quantum interference device (SQUID) magnetometer. Thermal analysis was carried out by DSC measurements, where the heating and cooling temperature rate was 10 K/min.

III. EXPERIMENTAL RESULTS

The Heusler $L2_1$-type structure is comprised of four interpenetrating fcc sublattices with A, B, C, and D sites. The A, B, C, and D sites are located at (0, 0, 0), (1/4, 1/4, 1/4), (1/2, 1/2, 1/2), and (3/4, 3/4, 3/4), respectively, as shown in Fig. 1. In the stoichiometric Heusler alloy Ni_2MnGa, Ni atoms occupy the A and C sites and the Mn atoms and Ga atoms the B and D sites, respectively.

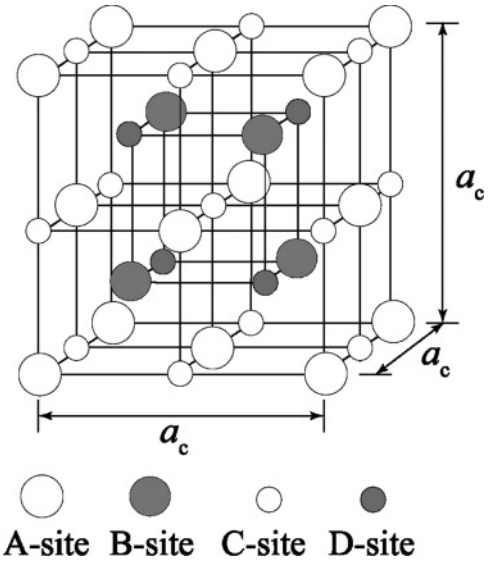

FIG. 1. Crystal structure of the Heusler-type alloy.

Figure 2(a) shows the observed x-ray powder diffraction pattern at room temperature of the sample with $x = 0.02$. Most of the diffraction lines can be indexed using an fcc structure. The intensities of the superlattice lines such as (111) and (200) agree well with the results calculated by assuming the $L2_1$ structure. These results indicate that the sample with $x = 0.02$ has the fully ordered $L2_1$ structure. As shown in Fig. 2(a), a few extra diffraction lines with very weak intensity were detected, indicating the existence of small amounts of other phase. The lattice parameter a_c of the sample with $x = 0.02$ is found to be 0.58203 nm. We observed similar x-ray powder diffraction patterns at room temperature for the samples with $x = 0.04$ and 0.06, indicating that the samples of $Ni_2MnGa_{1-x}Co_x$ alloys with the concentration range $0 \leqslant x \leqslant 0.06$ crystallize in the $L2_1$ structure at room temperature. The x-ray powder diffraction pattern of the sample with $x = 0.08$ is shown in Fig. 2(b). This x-ray powder diffraction pattern is similar to that in the martensite phase of FSMA $Ni_2MnGa_{0.88}Cu_{0.12}$.[17] The main reflections from $Ni_2MnGa_{0.88}Cu_{0.12}$ could be indexed using the tetragonal $D0_{22}$-type (space group: $I4/mmm$) structure. The fourteen-layered monoclinic ($14M$) structure (space group: $P2/m$) coexists with the tetragonal $D0_{22}$-type structure in $Ni_2MnGa_{0.88}Cu_{0.12}$. The only x-ray powder diffraction lines from the tetragonal phase were indexed as the $D0_{22}$-type structure in Fig. 2(b). We could not estimate the exact values of the lattice parameters and the volume of the sample with $x = 0.08$ because the strong diffraction lines from the tetragonal $D0_{22}$-type structure overlap with the diffraction lines from other structures. As the values of the atomic scattering factor for Ni, Mn, Co, and Ga atoms are close, we could not determine which site Co atoms in the $D0_{22}$-type structure preferentially occupy. Figure 2(c) shows the x-ray powder diffraction pattern at room temperature for the sample with $x = 0.13$. Most diffraction lines can be indexed with the tetragonal $D0_{22}$-type structure, where the a_t axis is chosen to be rotated in a c plane by 45° from the a_c axis in the $L2_1$ structure. The intensities of all diffraction lines agree well with the results calculated by assuming the $D0_{22}$-type structure as shown in the inset in

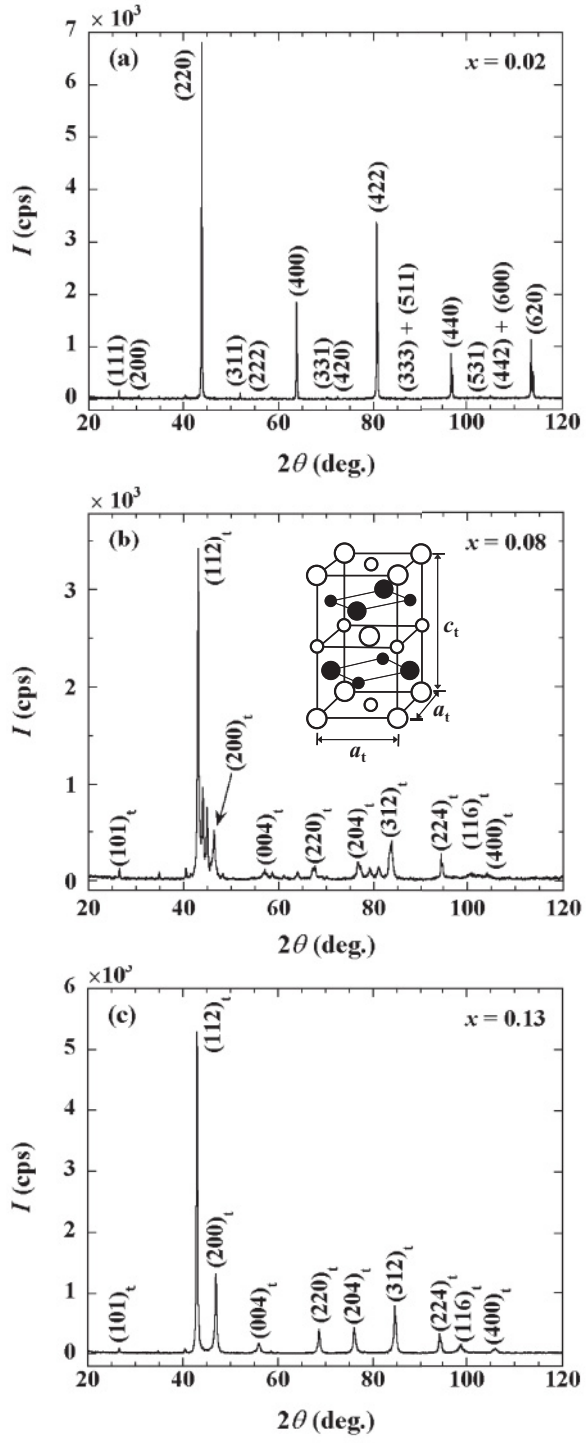

FIG. 2. X-ray powder diffraction patterns at room temperature of (a) $Ni_2MnGa_{0.98}Co_{0.02}$, (b) $Ni_2MnGa_{0.92}Co_{0.08}$, and (c) $Ni_2MnGa_{0.87}Co_{0.13}$. The inset in (b) shows the $D0_{22}$-type structure, where the symbols represent the four different sites A, B, C, and D.

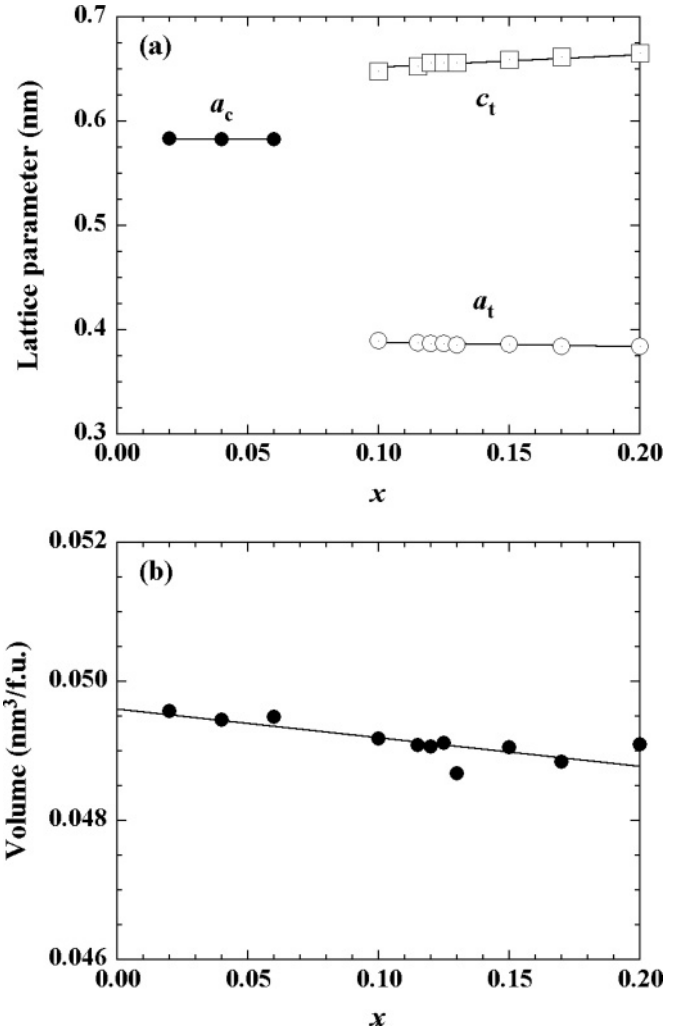

FIG. 3. Concentration dependence of (a) the lattice parameters and (b) the volume per formula unit for each structure of $Ni_2MnGa_{1-x}Co_x$ ($0 \leqslant x \leqslant 0.20$) alloys. Solid lines in the figures are guides for the eyes.

Fig. 2(b). The lattice parameters of the sample were estimated to be $a_t = 0.38518$ nm and $c_t = 0.65623$ nm, where the value of a_t is shorter by a factor $1/\sqrt{2}$ than a_c of the $L2_1$ structure in the absence of the lattice distortions. We observed similar x-ray powder diffraction patterns at room temperature for the samples with $x = 0.10$, 0.11, 0.115, 0.12, 0.15, 0.17, and 0.20, indicating that samples of $Ni_2MnGa_{1-x}Co_x$ alloys in the concentration range $0.10 \leqslant x \leqslant 0.20$ crystallize in the $D0_{22}$-type structure at room temperature. Figures 3(a) and 3(b) show the concentration dependence of the lattice parameters and volume per formula unit ($= 1/4\, a_c^3$) at room temperature of $Ni_2MnGa_{1-x}Co_x$ ($0 \leqslant x \leqslant 0.20$) alloys, respectively. As seen in Fig. 3(b), the volume per formula unit at room temperature decreases linearly with increasing x, which may be attributed to the difference in the ionic radii of the Co and Ga atoms. More recently, Li *et al.* calculated the equilibrium volume of $Ni_2MnGa_{1-x}Co_x$ alloys with the $L2_1$ structure by using the first-principles exact muffin-tin orbital method.[44] Their results are in good agreement with the experimental results shown in Fig. 3(a).

Figure 4(a) shows the temperature dependence of the initial permeability μ for the sample with $x = 0.02$. The arrows along the curves in this figure show the heating and cooling processes. The μ versus T curves of this sample are very similar to those of $Ni_2MnGa_{0.98}Cu_{0.02}$.[17] The abrupt increase of μ around 375 K with decreasing temperature corresponds

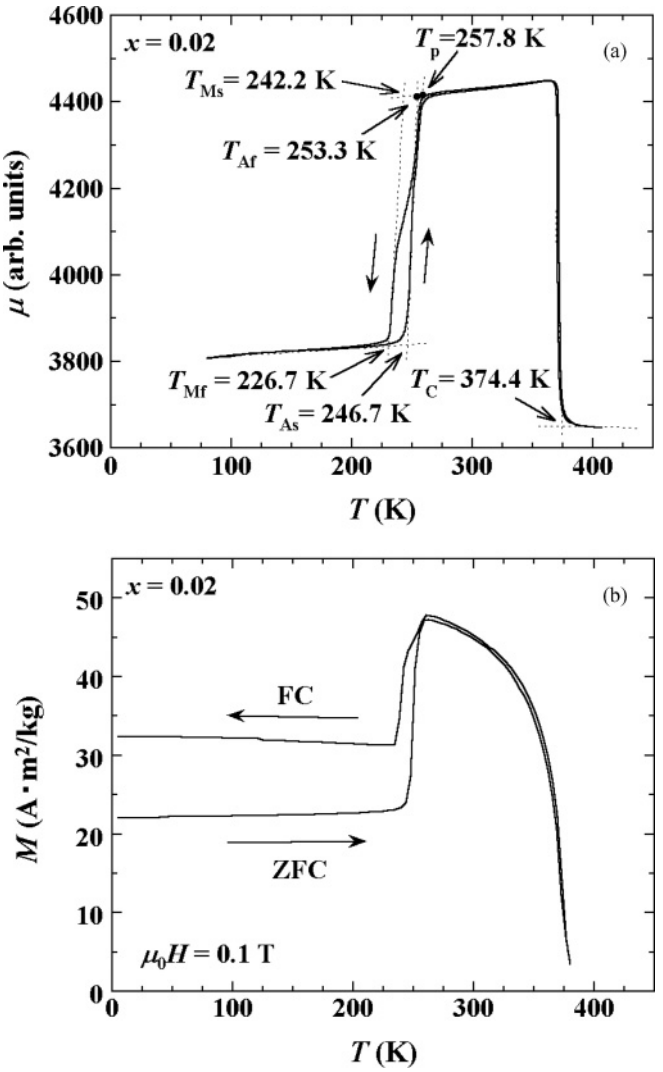

FIG. 4. Temperature dependence of (a) the initial permeability μ and (b) the magnetization M at 0.1 T for $Ni_2MnGa_{0.98}Co_{0.02}$. The arrows along the curves in (a) show the cooling and heating processes. T_C is the Curie temperature. T_{Ms} and T_{Mf} mean the martensitic transition starting temperature and the martensitic transition finishing temperature, respectively. T_{As} and T_{Af} represent the reverse martensitic transition starting temperature and the reverse martensitic finishing temperature, respectively. T_p shows the premartensitic transition temperature for the cooling and heating processes. The arrows with ZFC and FC along the curves in (b) show the ZFC and FC processes, respectively.

to the paramagnetic (Para) to ferromagnetic (Ferro) phase transition in the austenite region. The Curie temperature T_C was defined as the point of intersection following linear extrapolation of the higher and lower temperature ranges on the μ versus T curve. Using this method, T_C is found to be 374.4 K for the sample with $x = 0.02$. With further decrease in temperature, we observed an abrupt change of μ around 240 K with the thermal hysteresis. This abrupt change of μ corresponds to a martensitic transition. The martensitic transition starting and finishing temperatures T_{Ms} and T_{Mf} and the reverse martensitic transition starting and finishing temperatures T_{As} and T_{Af} were also defined as the points of the intersection of the linear extrapolation of both the higher and lower temperature ranges on the μ versus T curves as shown in the figure. As shown in Fig. 4(a), we observe an abrupt decrease of μ just above T_{Ms} with decreasing temperature. This abrupt decrease of μ corresponds to the premartensitic transition. Similar temperature dependence of μ around the premartensitic transition temperature T_P were observed for $Ni_2Mn_{0.95}Cu_{0.05}Ga$ and $Ni_2MnGa_{0.98}Cu_{0.02}$.[11,17] Figure 4(b) shows the temperature dependence of the magnetization M measured in zero-field-cooling (ZFC) and field-cooling (FC) processes in an applied field of 0.1 T for the sample with $x = 0.02$. In the ZFC process, the sample was first cooled to 5 K from room temperature under zero magnetic field, and the magnetic field of 0.1 T was applied at this temperature. Then, the magnetization was measured at this constant field with increasing temperature up to 383 K. After the magnetization measurement in the ZFC process, the magnetization measurement was carried out with decreasing temperature without removing the external field, i.e., in the FC process. As shown in Figs. 4(a) and 4(b), the martensitic transition is accompanied by the abrupt change of μ and M because the low symmetry of the martensite phase enhances the magnetocrystalline anisotropy energy, which forces magnetizations in martensitic variants to direct to their magnetic easy axes under the weak magnetic field 0.1 T.

Figures 5(a) and 5(b) show the temperature dependence of μ and M in 0.1 T for the sample with $x = 0.08$, respectively. The temperatures T_{Ms}, T_{Mf}, T_{As}, and T_{Af} of the sample with $x = 0.08$ were determined as shown in Fig. 5(a). It should be noted that the anomalous decrease of μ due to the premartensitic transition is not observed in the μ versus T curves for the sample with $x = 0.08$. Similar μ versus T and M versus T curves were observed for the samples with $x = 0.04$, 0.06, and 0.10. Figures 6(a) and 6(b) show the temperature dependence of μ and M at 0.1 T for the sample with $x = 0.13$. The μ versus T and M versus T curves in Figs. 6(a) and 6(b) are characteristic of ferromagnets with a ferromagnetic-paramagnetic second-order phase transition. As mentioned above, the x-ray powder diffraction pattern of the sample with $x = 0.13$ shows the martensite phase with the $D0_{22}$-type structure. To determine the martensitic transition temperature of the sample with $x = 0.13$, we carried out the DSC measurements. Figure 7 shows the DSC curves of the sample with $x = 0.13$ for the heating and cooling processes. T_{Ms}, T_{Mf}, T_{As}, and T_{Af} were determined by using the intersections of the baseline and the tangent lines with the largest slopes of the DSC peaks as shown in Fig. 7. Similar DSC curves were observed for the samples with $x = 0.15$, 0.17, and 0.20.

The experimental T versus x phase diagram of $Ni_2MnGa_{1-x}Co_x$ ($0 \leqslant x \leqslant 0.20$) alloys, which was constructed from the measurements of the temperature dependence of μ and M, and DSC measurements, is shown in Fig. 8. In the compositional interval $0 \leqslant x \leqslant 0.115$, the martensitic transition temperature T_M increases with increasing x, where T_M is defined as $T_M = (T_{Ms} + T_{Af})/2$. The premartensitic transition temperature T_P is observed in the compositional interval below $x \approx 0.04$. On the other hand, the Curie temperature is almost independent of x for the samples with $0 \leqslant x \leqslant 0.115$. With further increase of x, T_M increases almost linearly with

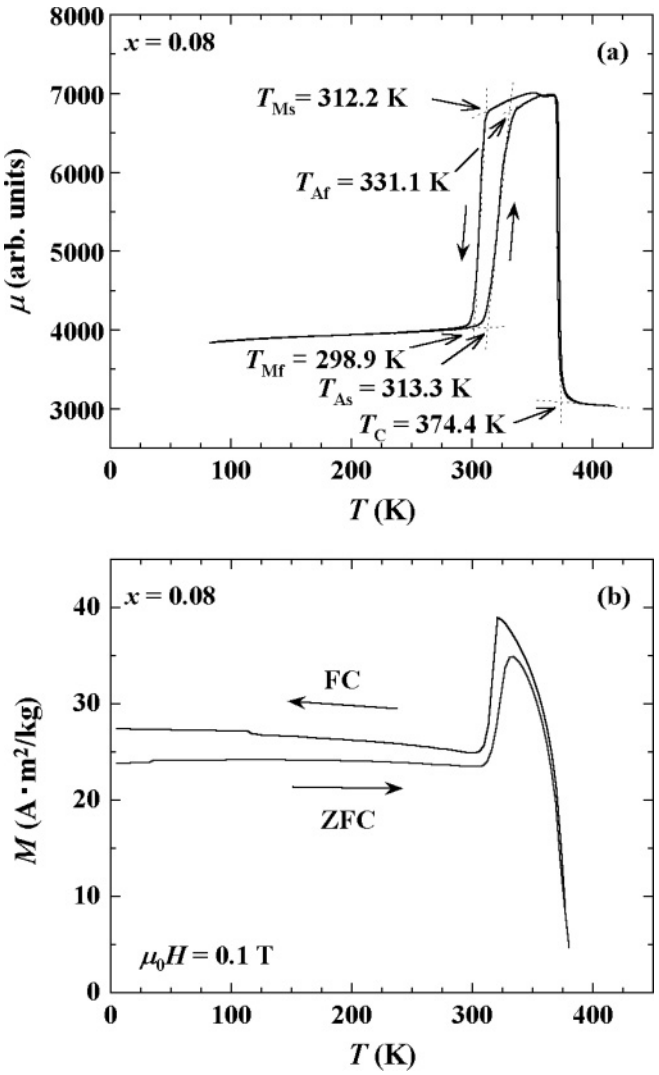

FIG. 5. Temperature dependence of (a) the initial permeability μ and (b) the magnetization M at 0.1 T for $Ni_2MnGa_{0.92}Cu_{0.08}$. The arrows along the curves in (a) show the cooling and heating processes. T_C is the Curie temperature. T_{Ms} and T_{Mf} mean the martensitic transition starting temperature and the martensitic transition finishing temperature, respectively. T_{As} and T_{Af} represent the reverse martensitic transition starting temperature and the reverse martensitic finishing temperature, respectively. The arrows with ZFC and FC along the curves in (b) show the ZFC and FC processes, respectively.

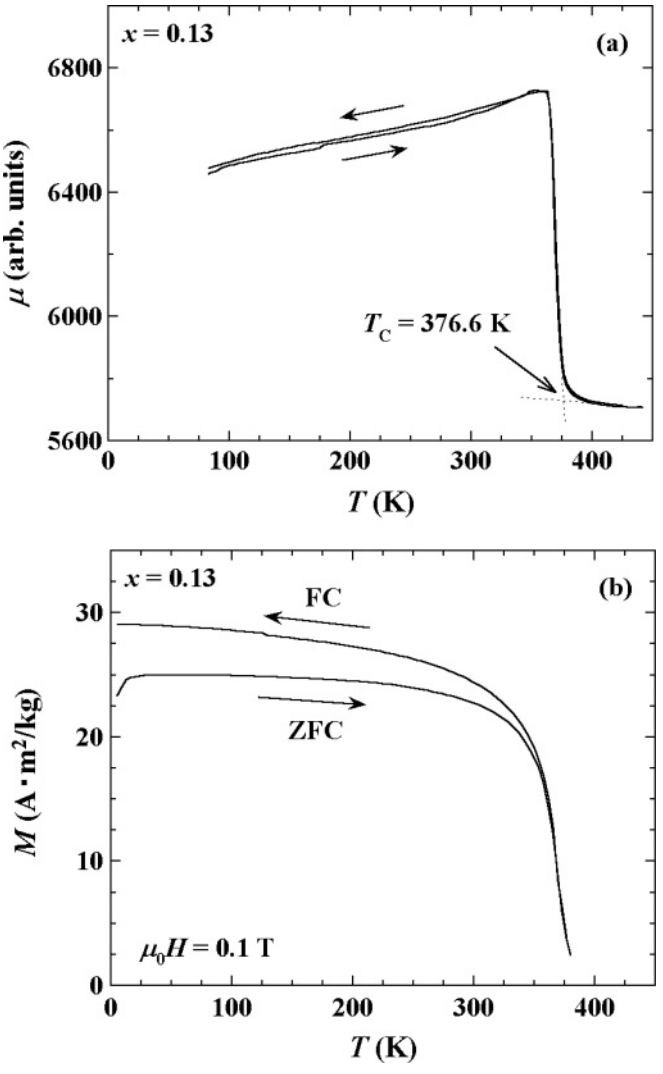

FIG. 6. Temperature dependence of (a) the initial permeability μ and (b) the magnetization M at 0.1 T for $Ni_2MnGa_{0.87}Co_{0.13}$. The arrows along the curves in (a) show the cooling and heating processes. T_C is the Curie temperature. The arrows with ZFC and FC along the curves in (b) show the ZFC and FC processes, respectively.

increasing x. On the other hand, in the compositional interval $0.115 \leqslant x \leqslant 0.20$, T_C decreases with increasing x. To sum up, two regions can be distinguished in the phase diagram shown in Fig. 8. In the first region, characterized by the Co concentration $0 \leqslant x \leqslant 0.115$, where $T_C > T_M$, the martensitic transition takes place between two ferromagnetic phases. The second region with $0.115 \leqslant x \leqslant 0.20$ is characterized by $T_C < T_M$, i.e., the ferromagnetic transition is in the martensite phase. The unusual characteristic of the phase diagram for $Ni_2MnGa_{1-x}Co_x$ ($0 \leqslant x \leqslant 0.20$) alloys shown in Fig. 8 is that T_C and T_M cross perfectly in the T versus x plane, and there appears no concentration region where T_C and T_M merge together. This phase diagram forms a contrast to those of $Ni_{2+x}Mn_{1-x}Ga$ ($0 \leqslant x \leqslant 0.36$), $Ni_2Mn_{1-x}Cu_xGa$ ($0 \leqslant x \leqslant 0.40$), and $Ni_2MnGa_{1-x}Cu_x$ ($0 \leqslant x \leqslant 0.25$) alloys, in which T_M and T_C can merge in their respective concentration regions. When, on the other hand, the phase diagram of $Ni_2MnGa_{1-x}Co_x$ ($0 \leqslant x \leqslant 0.20$) alloys obtained here is compared with that of $Ni_{50.6}Mn_{24.4}Ga_{25-x}Co_x$ ($0 \leqslant x \leqslant 6.4$) predicted by Soto-Parra *et al.*,[40] we note that both the two phase diagrams have no concentration region for the occurrence of the magnetostructural transition and are found to be similar to each other, except for the absence of the premartensite phase in the alloy system $Ni_{50.6}Mn_{24.4}Ga_{25-x}Co_x$.

Figure 9 shows the temperature dependence of M measured in the ZFC and the FC processes for $Ni_2MnGa_{0.96}Co_{0.04}$ ($x = 0.04$) at 0.1, 1, 2.5, and 5 T. As seen in Fig. 9, an abrupt increase of M on M versus T curves at T_M is observed in a field of 5 T in cooling and heating processes. At $\mu_0 H = 5$ T, M is saturated for $Ni_2MnGa_{0.96}Co_{0.04}$ (see Fig. 10). This implies that the magnetic moment per formula unit of the martensite phase is larger than that of the austenite phase.

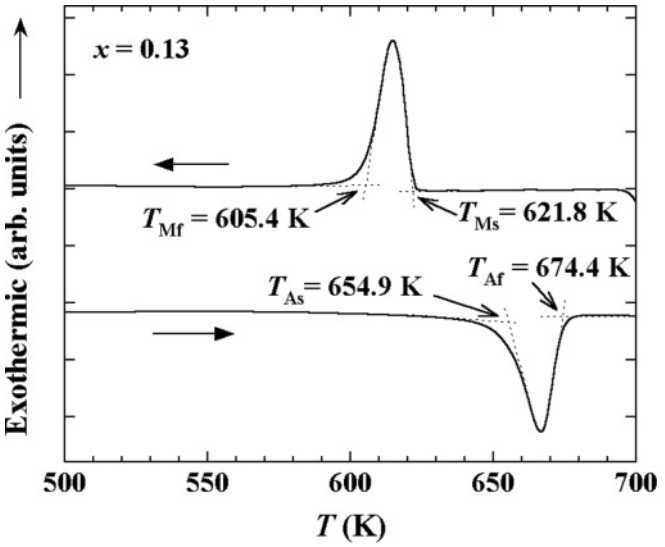

FIG. 7. DSC curves of $Ni_2MnGa_{0.87}Co_{0.13}$. The arrows along the curves show the cooling and heating processes. T_{Ms} and T_{Mf} mean the martensitic transition starting temperature and the martensitic transition finishing temperature, respectively. T_{As} and T_{Af} represent the reverse martensitic transition starting temperature and the reverse martensitic transition finishing temperature, respectively.

The magnetization curves at 5 K for $Ni_2MnGa_{1-x}Co_x$ ($0 \leqslant x \leqslant 0.20$) alloys with various concentrations x are shown in Fig. 10. The magnetization M at 5 K is saturated in a field of about 2 T. The spontaneous magnetization at 5 K for $Ni_2MnGa_{1-x}Co_x$ ($0 \leqslant x \leqslant 0.20$) alloys was determined by the linear extrapolation to $H/M = 0$ of the M^2 versus H/M curves. The magnetic moment per formula unit, μ_{tot}, at 5 K for

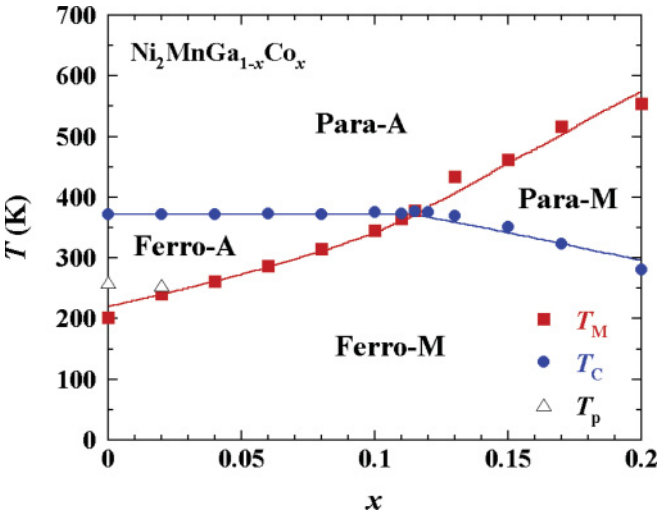

FIG. 8. (Color online) Phase diagram of $Ni_2MnGa_{1-x}Co_x$ ($0 \leqslant x \leqslant 0.20$) alloys. Para means paramagnetic state, and Ferro means ferromagnetic state. A and M represent the austenitic and martensitic states, respectively. T_C, T_M, and T_p are the Curie temperature, the martensitic transition temperature, and the premartensitic transition temperature, respectively. The data of the sample with $x = 0$ are taken from Ref. 10. Solid lines in the figure are the calculated results obtained by use of the parameter values given in the text (see Sec. IV).

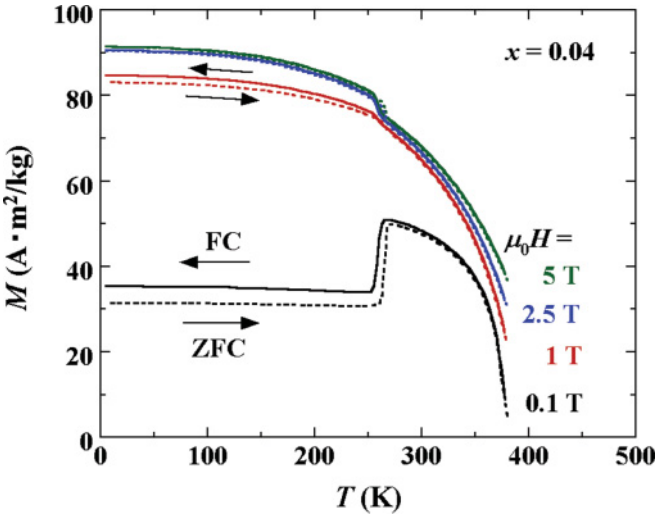

FIG. 9. (Color online) Temperature dependence of the magnetization M at 0.1, 1, 2.5, and 5 T for $Ni_2MnGa_{0.96}Co_{0.04}$. The dashed and solid lines show the ZFC and the FC processes, respectively.

$Ni_2MnGa_{1-x}Co_x$ ($0 \leqslant x \leqslant 0.20$) alloys was estimated from the spontaneous magnetization and is plotted against x as shown in Fig. 11. The μ_{tot} at 5 K of the stoichiometric Ni_2MnGa is estimated to be 3.96 μ_B/f.u. by extrapolation to $x = 0$ of the μ_{tot} versus x curve. Ahuja *et al.* carried out a magnetic Compton scattering study for the near-stoichiometric alloy $Ni_{2.03}Mn_{0.97}Ga$.[45] For $Ni_{2.03}Mn_{0.97}Ga$, they found the value of μ_{tot} to be 4.01 μ_B/f.u. at 110 K under 2 T. The value of the μ_{tot} at 5 K for Ni_2MnGa in this study is in excellent agreement with the value reported by Ahuja *et al.*[45] The μ_{tot} at 5 K decreases linearly with increasing x. Li *et al.* investigated the site preference and the magnetic moment of $Ni_2MnGa_{1-x}Co_x$ alloys with the $L2_1$ structure.[44] Their calculation indicates that Co atoms strongly prefer the Ni sublattice. The site occupancy of $Ni_2MnGa_{0.95}Co_{0.05}$ for the free-energy minimum was found to be $(Ni_{0.975}Co_{0.025})_2Mn(Ga_{0.95}Ni_{0.05})$. According to

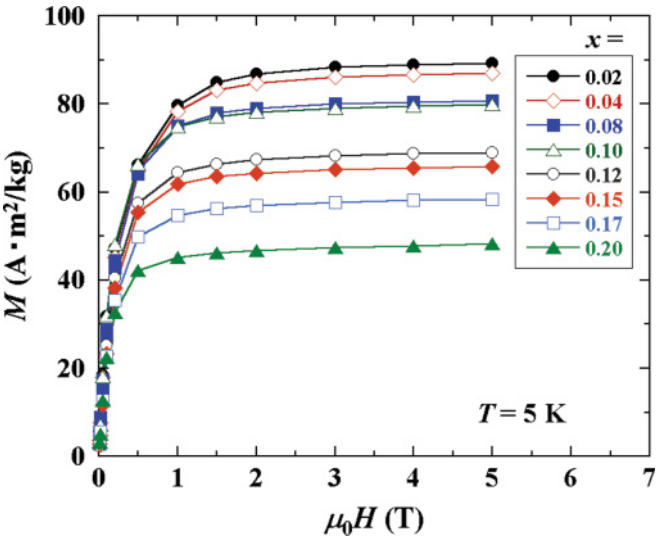

FIG. 10. (Color online) Magnetization curves at 5 K for $Ni_2MnGa_{1-x}Co_x$ alloys with various concentrations.

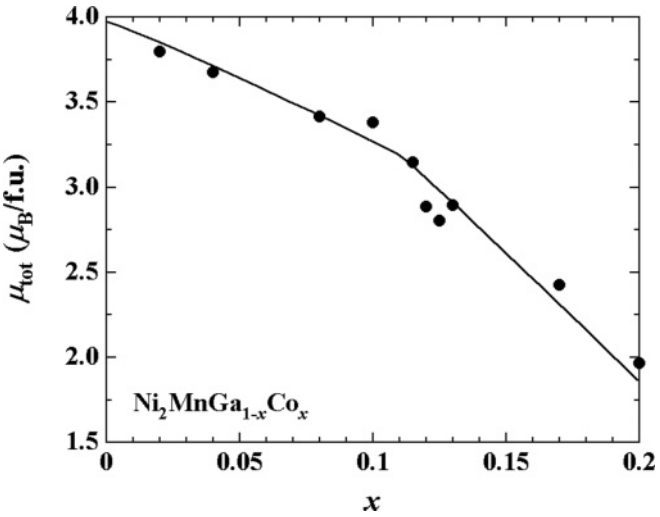

FIG. 11. Concentration dependence of the magnetic moment per formula unit, μ_{tot}, at 5 K for $Ni_2MnGa_{1-x}Co_x$ ($0 \leqslant x \leqslant 0.20$) alloys. The solid line is a guide for the eyes.

the results of calculation by Li *et al.*,[44] the magnetic moments of Co atoms on the Ni sublattice tend to be ferromagnetically coupled with those of Mn atoms on the Mn sublattice, and the magnetic moment of the Co atom on the Ni sublattice is estimated to be $1.03 \pm 0.02\ \mu_B$. It means that the increase of the concentration x for $Ni_2MnGa_{1-x}Co_x$ alloys leads to the increase of the magnetic moment per formula unit. However, as shown in Fig. 11, the magnetic moment per formula unit at 5 K of $Ni_2MnGa_{1-x}Co_x$ ($0 \leqslant x \leqslant 0.2$) alloys decreases with increasing x. We note that $Ni_2MnGa_{1-x}Co_x$ ($0 \leqslant x \leqslant 0.2$) alloys are in the martensite phase at 5 K. Furthermore, we observe the change of d μ_{tot}/dx around $x \approx 0.11$ as shown in Fig. 11. This concentration corresponds to the concentration of the cross over point of T_C and T_M in the phase diagram (see Fig. 8). It is not clear why the change of d μ_{tot}/dx appears around $x \approx 0.115$.

IV. PHENOMENOLOGICAL ANALYSES OF THE PHASE DIAGRAM

To find the reason for the unusual behavior of the observed phase boundaries, the phase diagram of $Ni_2MnGa_{1-x}Co_x$ ($0 \leqslant x \leqslant 0.20$) alloys is analyzed by use of the phenomenological Landau free energy. The premartensite phase, which is observed for $x \leqslant 0.03$, is out of the present analysis, since its order parameter is still open. All the other phases except for the premartensite phase are characterized by the two order parameters, i.e., the martensitic distortion e_3, which gives a tetragonal elongation $c/a > 1$ and the magnetization M. The free-energy $F(e_3, M)$ is expanded in powers of these order parameters so as to satisfy the crystal symmetry. As in many Landau theories, only the coefficients of ${e_3}^2$ and M^2 depend linearly on temperature T and concentration x. In order to make $F(e_3, M)$ tractable, e_3, M, and $F(e_3, M)$ are measured in their suitable units, being changed to $\overline{e}_3$, $\overline{M}$, and $\overline{F}(\overline{e}_3, \overline{M})$, respectively. As the result, the free energy is written as

$$\overline{F}(\overline{e}_3, \overline{M}) = \frac{1}{2}[t - t_c(x)]\overline{M}^2 + \frac{1}{4}\overline{M}^4 + r\left\{\frac{1}{2t_m(1)}[t - t_m(x)]\,\overline{e}_3^2 + \frac{2}{3}a\overline{e}_3^3 + \frac{1}{4}\overline{e}_3^4\right\} + \overline{F}_{int}(\overline{e}_3, \overline{M}), \quad (1)$$

where $\overline{F}_{int}(\overline{e}_3, \overline{M})$ is the energy of the interaction between $\overline{e_3}$ and $\overline{M}$ and is given by

$$\overline{F}_{int}(\overline{e}_3, \overline{M}) = \tfrac{1}{2}g\,\overline{e}_3^2\overline{M}^2 + \tfrac{1}{3}p\,\overline{e}_3^3\overline{M}^2. \quad (2)$$

In Eq. (1), temperatures were measured in units of the Curie temperature at $x = 0$, $T_C(0)$, so that

$$t = T/T_C(0), \quad (3)$$

and the real or fictitious second-order transition temperatures are expressed by

$$t_m(x) = t_m(0) + [t_m(1) - t_m(0)]x, \quad (4)$$

$$t_c(x) = 1 + [t_c(1) - 1]x. \quad (5)$$

The form of the free energy given by Eqs. (1)–(5) is the same as the one employed for $Ni_2Mn_{1-x}Cu_xGa$ ($0 \leqslant x \leqslant 0.40$) and $Ni_2MnGa_{1-x}Cu_x$ ($0 \leqslant x \leqslant 0.25$) alloys.[11,17]

The equilibrium $\overline{e}_3$ and $\overline{M}$ values are found by minimizing $\overline{F}(\overline{e}_3, \overline{M})$ with respect to these order parameters. The values of the coefficients in Eqs. (1), (2), (4), and (5) are chosen so that the calculated phase diagram may agree with the observed one. By analyzing the phase boundaries and comparing them with the experimental results, the following values are obtained.

$$t_c(1) = 1.0, \quad t_m(0) = -1.81, \quad t_m(1) = 4.65, \quad (6)$$

$$r = 0.760, \quad a = -0.706, \quad g = -0.607, \quad \text{and } p = 0.967. \quad (7)$$

The solid lines in Fig. 8 give the calculated phase diagram of $Ni_2MnGa_{1-x}Co_x$ ($0 \leqslant x \leqslant 0.20$) alloys. As seen in this figure, the agreement between theory and experiment is satisfactory. In particular, the theory reproduces the following observed facts. The phase boundary line between the Para-A and ferromagnetic austenite (Ferro-A) phases and its extrapolation crosses with that between the Para-A and paramagnetic martensite (Para-M) phases and its extrapolation. Near the crossing point, namely, (x_A, t_A), the phase diagram exhibits neither a magnetostructural transition nor reentrant ferromagnetism. At concentrations above x_A, the phase boundary line between the Para-M and Ferro-M phases is pushed downward from the extrapolated boundary line between the Para-A and Ferro-A phases in the martensite phase, while at concentrations below x_A, the phase boundary line between the Ferro-A and Ferro-M phases is pushed upward from the extrapolated boundary line between the Para-A and Para-M phases in the ferromagnetic phase. In other words, above x_A, $\overline{e}_3$ and $\overline{M}$ are repulsive to one another, but below x_A, they are attractive through the interaction energy given by Eq. (2). This characteristic of $Ni_2MnGa_{1-x}Co_x$ ($0 \leqslant x \leqslant 0.20$) alloys is compared with the attraction in $Ni_{2+x}Mn_{1-x}Ga$ ($0 \leqslant x \leqslant 0.36$) and $Ni_2Mn_{1-x}Cu_xGa$ ($0 \leqslant x \leqslant 0.40$) alloys and the

repulsion in $Ni_2Mn_{1+x}Z_{1-x}$ (Z = In, Sn and Sb) alloys in the whole region of concentration.[11]

The crossover from the repulsive interaction to the attractive one occurs via a cancellation of the two terms on the right-hand side of Eq. (2) by changing x. Even as this cancellation is realized at a point (x, t), the two order parameters do not interfere with each other. From this fact, the condition for the crossing of the boundary line between the Para-A and Ferro-A phases and that between the Para-A and Para-M phases can be found as follows. From Eq. (1), it is shown that the martensitic transition is of first order and takes place at the transition temperature $t_m(x) + (8/9)a^2$ in the paramagnetic state. Furthermore, it is also shown that the equilibrium martensitic distortion at this transition temperature, $\bar{e}_{3,\mathrm{A-M}}$, is given by

$$\bar{e}_{3,\mathrm{A-M}} = -(4/3)a. \tag{8}$$

We note that the distortion at the martensitic transition temperature is independent of x, although the martensitic distortion below its transition temperature changes with x. Equations (8) and (2) prove that the two terms can cancel each other at the temperatures of the martensitic transition when

$$p = \frac{9g}{8a}. \tag{9}$$

So long as the quantities a, g, and p satisfy this condition, then the perfect crossing occurs irrespective of the crossing point (x_A, t_A). This is the case that happens in $Ni_2MnGa_{1-x}Co_x$ ($0 \leqslant x \leqslant 0.20$) alloys.

The above success in the explanation of the phase diagram states that the strikingly different features of the phase diagrams of the alloy systems with the magnetostructural transition and the present alloy system with no matgnetostructural transition is ascribed only to the difference in the relative strength of the second term to that of the first term on the right-hand side of Eq. (2). In turn, this result further states that the phenomenological free energy proposed in Ref. 11 can be suitable for the alloy systems investigated hitherto and points the way to find any microscopic origin of the two phase transitions and their interplay.

V. CONCLUSION

Magnetization, initial permeability and DSC measurements were carried out on the FSMAs $Ni_2MnGa_{1-x}Co_x$ ($0 \leqslant x \leqslant 0.20$). On the basis of the experimental results, the phase diagram of $Ni_2MnGa_{1-x}Co_x$ ($0 \leqslant x \leqslant 0.20$) alloys was determined. In the compositional range below $x \approx 0.115$, T_C was found to be independent of the concentration x. On the other hand, T_M increases with increasing x in the compositional interval $0 \leqslant x \leqslant 0.20$. In the compositional range $0.115 \leqslant x \leqslant 0.20$, T_C decreases with increasing x. An unusual characteristic of the phase diagram for $Ni_2MnGa_{1-x}Co_x$ ($0 \leqslant x \leqslant 0.20$) alloys is that T_C and T_M cross perfectly in the T versus x plane without merging together.

In order to understand the phase diagram observed for $Ni_2MnGa_{1-x}Co_x$ ($0 \leqslant x \leqslant 0.20$) alloys, we used a Landau-type phenomenological theory. The analysis showed that the biquadratic coupling term, together with a higher-order coupling term, of the martensitic distortion to the magnetization plays an important role in the interplay between the martensite phase and the ferromagnetic phase. It was shown that the crossing of T_C and T_M results from a cancellation of the biquadratic and higher-order coupling terms.

ACKNOWLEDGMENTS

The authors would like to express sincere thanks to K. Obara of the Institute for Materials Research, Tohoku University, for his help in the sample preparation. This work was partly supported by a Grant-in-Aid for Scientific Research from the Japan Society for the Promotion of Science (JSPS)/MEXT.

*rieume@imr.tohoku.ac.jp

[1] K. Ullakko, J. K. Huang, C. Kantner, R. C. O'Handley, and V. V. Kokorin, Appl. Phys. Lett. **69**, 1966 (1996).
[2] A. Sozinov, A. A. Likhachev, N. Lanska, and K. Ullakko, Appl. Phys. Lett. **80**, 1746 (2002).
[3] A. A. Cherechukin, T. Takagi, M. Matsumoto, and V. D. Buchel'nikov, Phys. Lett. A **326**, 146 (2004).
[4] F. Albertini, F. Canepa, S. Cirafici, E. A. Franceschi, M. Napoletano, A. Paoluzi, L. Pareti, and M. Solzi, J. Magn. Magn. Mater. **272–276**, 2111 (2004).
[5] M. Pasquale, C. P. Sasso, L. H. Lewis, L. Giudici, T. Lograsso, and D. Schlagel, Phys. Rev. B **72**, 094435 (2005).
[6] F. Albertini, M. Solzi, A. Paoluzi, and L. Righi, Mater. Sci. Forum **583**, 169 (2008).
[7] A. Planes, L. Mañosa, and M. Acet, J. Phys.: Condens. Matter **21**, 233201 (2009).
[8] L. Caron, N. T. Trung, and E. Brück, Phys. Rev. B **84**, 020414(R) (2011).
[9] P. J. Webster, K. R. A. Ziebeck, S. L. Town, and M. S. Peak, Philos. Mag. B **49**, 295 (1984).
[10] P. J. Brown, J. Crangle, T. Kanomata, M. Matsumoto, K.-U. Neumann, B. Ouladdiaf, and K. R. A. Ziebeck, J. Phys.: Condens. Matter **14**, 10159 (2002).
[11] M. Kataoka, K. Endo, N. Kudo, T. Kanomata, H. Nishihara, T. Shishido, R. Y. Umetsu, M. Nagasako, and R. Kainuma, Phys. Rev. B **82**, 214423 (2010).
[12] V. V. Khovaylo, V. D. Buchelnikov, R. Kainuma, V. V. Koledov, M. Ohtsuka, V. G. Shavrov, T. Takagi, S. V. Taskaev, and A. N. Vasiliev, Phys. Rev. B **72**, 224408 (2005).
[13] P. Entel, V. D. Buchelnikov, V. V. Khovailo, A. T. Zayak, W. A. Adeagbo, M. E. Gruner, H. C. Herper, and E. F. Wassermann, J. Phys. D: Appl. Phys. **39**, 865 (2006).
[14] A. M. Gomes, M. Khan, S. Stadler, N. Ali, I. Dubenko, A. Y. Takeuchi, and A. P. Guimarães, J. Appl. Phys. **99**, 08Q106 (2006).
[15] S. Stadler, M. Khan, J. Mitchell, N. Ali, A. M. Gomes, I. Dubenko, A. Y. Takeuchi, and A. P. Guimarães, Appl. Phys. Lett. **88**, 192511 (2006).
[16] B. R. Gautam, I. Dubenko, J. C. Mabon, S. Stadler, and N. Ali, J. Alloys Compd. **472**, 35 (2009).

[17]K. Endo, T. Kanomata, A. Kimura, M. Kataoka, H. Nishihara, R. Y. Umetsu, K. Obara, T. Shishido, M. Nagasako, R. Kainuma, and K. R. A. Ziebeck, Mater. Sci. Forum **684**, 165 (2011).
[18]P. Entel, M. E. Gruner, W. A. Adeagbo, and A. T. Zayak, Mater. Sci. Eng. A **481 & 482**, 258 (2008).
[19]H. Nakamura, K. Tsuchiya, and M. Umemoto, Trans. Mater. Res. Soc. Jpn. **26**, 287 (2001).
[20]V. V. Khovailo, T. Abe, V. V. Koledov, M. Matsumoto, H. Nakamura, R. Note, M. Ohtsuka, V. G. Shavrov, and T. Takagi, Mater. Trans. **44**, 2509 (2003).
[21]V. V. Khovailo, V. A. Chernenko, A. A. Cherechukin, T. Takagi, and T. Abe, J. Magn. Magn. Mater. **272–276**, 2067 (2004).
[22]Y. Katano, M. Ohtsuka, M. Matsumoto, K. Koike, and K. Itagaki, Mater. Trans. **45**, 350 (2004).
[23]S. Guo, Y. Zhang, B. Quan, J. Li, Y. Qi, and X. Wang, Smart Mater. Struct. **14**, S236 (2005).
[24]M. Khan, I. Dubenko, S. Stadler, and N. Ali, J. Appl. Phys. **97**, 10M304 (2005).
[25]I. Glavatskyy, N. Glavatska, O. Söderberg, S.-P. Hannula, and J.-U. Hoffmann, Scr. Mater. **54**, 1891 (2006).
[26]M. Khan, S. Stadler, and N. Ali, J. Appl. Phys. **99**, 08M705 (2006).
[27]S. Y. Yu, Z. X. Cao, L. Ma, G. D. Liu, J. L. Chen, G. H. Wu, B. Zhang, and X. X. Zhang, Appl. Phys. Lett. **91**, 102507 (2007).
[28]M. Khan, I. Dubenko, S. Stadler, and N. Ali, J. Appl. Phys. **102**, 023901 (2007).
[29]V. Sánchez-Alarcos, J. I. Pérez-Landazábal, V. Recarte, C. Gómez-Polo, and J. A. Rodríguez-Velamazán, Acta Mater. **56**, 5370 (2008).
[30]D. Y. Cong, S. Wang, Y. D. Wang, Y. Ren, L. Zuo, and C. Esling, Mater. Sci. Eng. A **473**, 213 (2008).
[31]V. Sánchez-Alarcos, J. I. Pérez-Landazábal, and V. Recarte, Mater. Sci. Eng. A **481 & 482**, 293 (2008).
[32]L. Ma, H. W. Zhang, S. Y. Yu, Z. Y. Zhu, J. L. Chen, G. H. Wu, H. Y. Liu, J. P. Qu, and Y. X. Li, Appl. Phys. Lett. **92**, 032509 (2008).
[33]Y. Ma, S. Yang, C. Wang, and X. Liu, Scr. Mater. **58**, 918 (2008).
[34]S. Fabbrici, F. Albertini, A. Paoluzi, F. Bolzoni, R. Cabassi, M. Solzi, L. Righi, and G. Calestani, Appl. Phys. Lett. **95**, 022508 (2009).
[35]T. Kanomata, Y. Kitsunai, K. Sano, Y. Furutani, H. Nishihara, R. Y. Umetsu, R. Kainuma, Y. Miura, and M. Shirai, Phys. Rev. B **80**, 214402 (2009).
[36]Y. Ma, S. Yang, Y. Liu, and X. Liu, Acta Mater. **57**, 3232 (2009).
[37]K. Rolfs, M. Chmielus, R. C. Wimpory, A. Mecklenburg, P. Müllner, and R. Schneider, Acta Mater. **58**, 2646 (2010).
[38]B. M. Wang, P. Ren, Y. Liu, and L. Wang, J. Magn. Magn. Mater. **322**, 715 (2010).
[39]S. Yan, J. Pu, B. Chi, and L. Jian, J. Alloys Compd. **507**, 331 (2010).
[40]D. E. Soto-Parra, X. Moya, L. Mañosa, A. Planes, H. Flores-Zúñiga, F. Alvarado-Hernández, R. A. Ochoa-Gamboa, J. A. Matutes-Aquino, and D. Ríos-Jara, Philos. Mag. **90**, 2771 (2010).
[41]P. O. Castillo-Villa, D. E. Soto-Parra, J. A. Matutes-Aquino, R. A. Ochoa-Gamboa, A. Planes, L. Mañosa, D. González-Alonso, M. Stipcich, R. Romero, D. Ríos-Jara, and H. Flores-Zúñiga, Phys. Rev. B **83**, 174109 (2011).
[42]S. Fabbrici, J. Kamarad, Z. Arnold, F. Casoli, A. Paoluzi, F. Bolzoni, R. Cabassi, M. Solzi, G. Porcari, C. Pernechele, and F. Albertini, Acta Mater. **59**, 412 (2011).
[43]F. Albertini, S. Fabbrici, A. Paoluzi, J. Kamarad, Z. Arnold, L. Righi, M. Solzi, G. Porcari, C. Pernechele, D. Serrate, and P. Algarabel, Mater. Sci. Forum, **684**, 151 (2011).
[44]C. M. Li, H. B. Luo, Q. M. Hu, R. Yang, B. Johansson, and L. Vitos, Phys. Rev. B **84**, 024206 (2011).
[45]B. L. Ahuja, B. K. Sharma, S. Mathur, N. L. Heda, M. Itou, A. Andrejczuk, Y. Sakurai, A. Chakrabarti, S. Banik, A. M. Awasthi, and S. R. Barman, Phys. Rev. B **75**, 134403 (2007).